

A new determination of the $\gamma\pi \rightarrow \pi\pi$ anomalous amplitude via $\pi^-e^- \rightarrow \pi^-e^-\pi^0$ data

I. Giller,^{1,*} A. Ocherashvili,^{1,†} T. Ebertshäuser,^{2,‡} M. A. Moinester,^{1,§} and S. Scherer^{2,¶}

¹*School of Physics and Astronomy,
Raymond and Beverly Sackler Faculty of Exact Sciences,
Tel Aviv University, 69978 Tel Aviv, Israel*

²*Institut für Kernphysik, Johannes Gutenberg-Universität,
J. J. Becher-Weg 45, D-55099 Mainz, Germany*

(Dated: March 21, 2005)

Abstract

We discuss the reaction $\pi^-e^- \rightarrow \pi^-e^-\pi^0$ with the purpose of obtaining information on the $\gamma\pi \rightarrow \pi\pi$ anomalous amplitude $\mathcal{F}_{3\pi}$. We compare a full calculation at $\mathcal{O}(p^6)$ in chiral perturbation theory and various phenomenological predictions with the existing data of Amendolia *et al.* By integrating our theory results using Monte Carlo techniques we obtain $\sigma = 2.05$ nb at $\mathcal{O}(p^6)$ and $\sigma = 2.17$ nb after including the dominant electromagnetic correction. Both results are in good agreement with the experimental cross section of $\sigma = (2.11 \pm 0.47)$ nb. On the basis of the ChPT results one would extract from the the experimental cross section as amplitudes $\mathcal{F}_{3\pi}^{(0)\text{extr}} = (9.9 \pm 1.1)$ GeV^{-3} and $\mathcal{F}_{3\pi}^{(0)\text{extr}} = (9.6 \pm 1.1)$ GeV^{-3} , respectively, which have to be compared with the low-energy theorem $\mathcal{F}_{3\pi} = e/(4\pi^2 F_\pi^3) = 9.72 \text{ GeV}^{-3}$. We emphasize the need for new data to allow for a comparison of experimental and theoretical distributions and to obtain $\mathcal{F}_{3\pi}$ with smaller uncertainty.

PACS numbers: 11.30.Rd,13.60.Le

*Present address: Parametric Technology Israel Ltd., 37 Havazelet Hasharon St., Beit Noy, 46641 Herzlia, Israel

†Present address: Advanced Technology Center, Sheba Medical Center, Tel Hashomer, 52621 Ramat Gan, Israel

‡Present address: Deutsche Forschungsgemeinschaft, Kennedyallee 40, D-53175 Bonn, Germany

§Electronic address: murraym@tauphy.tau.ac.il

¶Electronic address: scherer@kph.uni-mainz.de

I. INTRODUCTION AND OVERVIEW

Ever since the late 1960s anomalies [1, 2, 3, 4] have played an important role in our understanding of strong-interaction physics. Anomalies arise if the symmetries of the Lagrangian at the classical level are not supported by the quantized theory after renormalization, resulting in so-called anomalous Ward identities [3]. For the case of chiral $SU(3)_L \times SU(3)_R$, the constraints due to the anomalous Ward identities have efficiently been taken care of through the effective Wess-Zumino-Witten (WZW) action [5, 6]. The WZW action is expressed in terms of the pseudoscalar octet of Goldstone bosons and contributes at $\mathcal{O}(p^4)$ in the momentum expansion of chiral perturbation theory [7] (for an overview see, e.g., Refs. [8, 9]). It is determined through the underlying group structure up to an overall constant [5] and, in the purely strong sector, gives rise to interaction vertices involving an odd number of Goldstone bosons (odd-intrinsic-parity sector) [6]. Using topological arguments, Witten has shown that the WZW action is quantized, i.e. a multiple of an integer parameter n . By including a coupling to electromagnetism, this parameter has been identified as the number of colors N_c by comparing with the prediction of the QCD triangle diagram for the (anomalous) decay $\pi^0 \rightarrow \gamma\gamma$. Once the overall factor is fixed, the (gauged) WZW action also predicts other interactions such as the $\gamma\pi^+\pi^0\pi^-$ vertex. However, it has recently been pointed out by Bär and Wiese [10] that the N_c dependence in the pion-photon vertices is completely canceled once the N_c dependence of the quark charges is consistently taken into account. In that sense, the width of the decay $\pi^0 \rightarrow \gamma\gamma$ is predicted absolutely without reference to the number of colors. The conclusion from their analysis is that one should rather consider three-flavor processes such as $\eta \rightarrow \pi^+\pi^-\gamma$ or $K\gamma \rightarrow K\pi$ to test the expected N_c dependence [10, 11] in a low-energy reaction. However, by investigating the corresponding η and η' decays up to next-to-leading order in the framework of the combined $1/N_c$ and chiral expansions, Borasoy and Lipartia have concluded that the number of colors cannot be determined from these decays due to the importance of sub-leading terms which are needed to account for the experimental decay widths and photon spectra [12].

The decay $\pi^0 \rightarrow \gamma\gamma$ is the prime example of an anomalous process [1, 4] and its invariant amplitude can be written as

$$\mathcal{M}_{\pi^0 \rightarrow \gamma\gamma} = i\mathcal{F}_\pi(M_{\pi^0}^2)\epsilon_{\mu\nu\rho\sigma}q_1^\mu\epsilon_1^{\nu*}q_2^\rho\epsilon_2^{\sigma*}, \quad \epsilon_{0123} = 1. \quad (1)$$

The prediction in the chiral limit, as obtained from the WZW action, is given by [5, 6, 10]

$$\mathcal{F}_\pi(0) = \frac{\alpha}{\pi F_0}, \quad (2)$$

where $\alpha = e^2/4\pi \approx 1/137$, $e > 0$, and F_0 denotes the $SU(3)$ chiral limit of the pion-decay constant [7]: $F_\pi = F_0[1 + \mathcal{O}(m_q)] = 92.4 \text{ MeV}$ [13]. Using Eq. (2) with the empirical value F_π instead of F_0 , one obtains for the decay rate

$$\Gamma_{\pi^0 \rightarrow \gamma\gamma} = \frac{\alpha^2 M_{\pi^0}^3}{64\pi^3 F_\pi^2} = 7.73 \text{ eV} \quad (3)$$

in agreement with the average value of Ref. [13]:

$$\Gamma_{\pi^0 \rightarrow \gamma\gamma} = (7.74 \pm 0.55) \text{ eV}. \quad (4)$$

Corrections due to explicit chiral symmetry breaking have been studied in Refs. [14, 15, 16, 17, 18, 19]. The most recent analyses yield $(8.06 \pm 0.02 \pm 0.06) \text{ eV}$ [17] in $SU(2)_L \times$

$SU(2)_R$ chiral perturbation theory at $\mathcal{O}(p^6)$ including electromagnetic corrections at $\mathcal{O}(e^2 p^4)$, (8.60 ± 0.10) eV [18] in the framework of a dispersion theory approach, and (8.10 ± 0.08) eV [19] using $U(3)_L \times U(3)_3$ chiral perturbation theory at $\mathcal{O}(p^6)$ in combination with large- N_c arguments. As has been stressed in Ref. [19], the individual experimental results show a large dispersion and depend on the specific reaction used to extract the amplitude. The Primakoff Experiment at Jefferson Lab (PrimEx) [20] aims at a determination of the width with an accuracy of 1.5 % and will thus match the increased precision of the theoretical analysis.

As mentioned above, the WZW action also predicts more complicated processes such as the $\gamma\pi^+\pi^0\pi^-$ interaction and one clearly needs to confirm our picture of both the leading-order term as well as the relevant corrections. The invariant amplitude for $\gamma^*(q) + \pi^-(p_b) \rightarrow \pi^0(p_2) + \pi^-(p_3)$ can be written as

$$\mathcal{M}_{\gamma\pi^- \rightarrow \pi^0\pi^-}(q, p_b; p_2, p_3) = -i\mathcal{F}_{3\pi}(s_2, t_2, u_2; q^2)\epsilon_{\mu\nu\rho\sigma}\epsilon^\mu p_b^\nu p_2^\rho p_3^\sigma, \quad (5)$$

where the Mandelstam variables are defined as $s_2 = (q + p_b)^2$, $t_2 = (p_b - p_3)^2$, $u_2 = (p_b - p_2)^2$ and satisfy the standard relation $s_2 + u_2 + t_2 = 2M_{\pi^-}^2 + M_{\pi^0}^2 + q^2$.¹ The lowest-order prediction [$\mathcal{O}(p^4)$] is independent of s_2 , t_2 , u_2 , and q^2 [5, 6, 21],

$$\mathcal{F}_{3\pi} = \frac{e}{4\pi^2 F_0^3} \approx \frac{e}{4\pi^2 F_\pi^3} = 9.72 \text{ GeV}^{-3}. \quad (6)$$

The physical threshold for $q^2 = 0$ is at $s_2^{\text{thr}} = (M_{\pi^-} + M_{\pi^0})^2$, $t_2^{\text{thr}} = -M_{\pi^-} M_{\pi^0}^2 / (M_{\pi^-} + M_{\pi^0})$, and $u_2^{\text{thr}} = M_{\pi^-} (M_{\pi^-}^2 - M_{\pi^-} M_{\pi^0} - M_{\pi^0}^2) / (M_{\pi^-} + M_{\pi^0})$.

The amplitude $\mathcal{F}_{3\pi}$ was measured by Antipov *et al.* [22] at Serpukhov using 40 GeV pions. Their study involved pion pair production by pions in the nuclear Coulomb field via the Primakoff reaction

$$\pi^- + (Z, A) \rightarrow \pi^{-'} + (Z, A) + \pi^0, \quad (7)$$

where Z and A denote the nuclear charge and mass number, respectively. In the one-photon-exchange domain, Eq. (7) is equivalent to

$$\pi^- + \gamma^* \rightarrow \pi^{-'} + \pi^0 \quad (8)$$

with an almost real photon ($q^2 \approx 0$). Diffractive production of the two-pion final state is blocked by G -parity conservation. At CERN COMPASS [23], a physics program based on pion and kaon scattering from the nuclear Coulomb field (Primakoff scattering [24]) has begun. The program goals include state-of-the-art measurements of the chiral anomaly transitions $\pi^- + \gamma^* \rightarrow \pi^{-'} + \pi^0$ and $K^- + \gamma^* \rightarrow K^{-'} + \pi^0$ as well as measurements of pion and kaon polarizabilities and radiative transitions [25] and hybrid meson production [26].

The chiral anomaly sample of Ref. [22] (roughly 200 events) covered the ranges $s_2 < 10 M_\pi^2$ and $|t_2| < 3.5 M_\pi^2 < s_2$. The small t_2 range selects events predominantly associated with the exchange of a virtual photon, for which the target nucleus acts as a spectator. Assuming a constant amplitude $\mathcal{F}_{3\pi}$, the value

$$\mathcal{F}_{3\pi}^{\text{exp}} = (12.9 \pm 0.9 \pm 0.5) \text{ GeV}^{-3} \quad (9)$$

¹ Our notation and kinematics will be discussed in more detail in Sec. II.

was extracted from the experiment [22]. The considerable discrepancy with the theoretical prediction of Eq. (6) has generated a lot of interest in clarifying the situation from both the experimental and theoretical sides.

Higher-order corrections in the odd-intrinsic-parity sector of ChPT have extensively been studied by Bijmens *et al.* [15, 27, 28, 29]. They included one-loop diagrams involving one vertex from the WZW term and tree diagrams from the anomalous $\mathcal{O}(p^6)$ Lagrangian [30, 31, 32], where the parameters of the Lagrangian have been estimated via vector-meson dominance (VMD) calculations. While the higher-order corrections to \mathcal{F}_π of Eq. (2) are small, for $\mathcal{F}_{3\pi}$ they increase the lowest-order value between 7 % and 12 % within the kinematic range of the Serphukov experiment [28]. Moreover, genuine one-loop corrections and $\mathcal{O}(p^6)$ tree-level contributions were found to be comparable in size. It has also been stressed by Holstein [33] that the experimental value of Eq. (9) was obtained under the assumption of a *constant* amplitude whereas a re-analysis using a suitable dependence on the kinematical variables would produce a lower value [33]

$$\mathcal{F}_{3\pi}^{\text{exp}} = (11.9 \pm 0.9 \pm 0.5) \text{ GeV}^{-3}, \quad (10)$$

and thus reduce the difference between theory and experiment. A sophisticated analysis has been carried out by Hannah [34] in the framework of a two-loop evaluation [$\mathcal{O}(p^8)$] using dispersive methods. From a comparison with the Antipov *et al.* data with the two-loop analysis leaving $\mathcal{F}_{3\pi}^{(0)}$ as a free parameter, Hannah obtained

$$\mathcal{F}_{3\pi}^{\text{exp}} = (11.4 \pm 1.3) \text{ GeV}^{-3}. \quad (11)$$

By also including radiative corrections, Ametller *et al.* [35] showed that the electromagnetic corrections generate a sizeable increase in the Primakov cross section, leading, in comparison with Eq. (11), to a further decrease

$$\mathcal{F}_{3\pi}^{\text{exp}} = (10.7 \pm 1.2) \text{ GeV}^{-3}. \quad (12)$$

Finally, using an integral equation approach, Truong [36] obtained

$$\mathcal{F}_{3\pi} = 11.2 \text{ GeV}^{-3}. \quad (13)$$

Further theoretical investigations of $\mathcal{F}_{3\pi}$ include calculations in the framework of dynamical constituent quarks [37].

The limited accuracy of the existing data in combination with the various new calculations clearly motivates improved and more precise experiments [23, 38, 39]. In a recent JLab experiment [39], results on $\gamma \rightarrow 3\pi$ were obtained from an analysis of $\gamma p \rightarrow \pi^+ \pi^0 n$ data taken with the CLAS detector. The photon energy was approximately 2 GeV. A Chew-Low analysis was used to extract $\mathcal{F}_{3\pi}$ from the cross sections over a large kinematic range. Preliminary results were presented by B. Asavapibhop [40] and an experimental paper is in preparation [41].

In this present work, we will focus on the reaction

$$\pi^- + e^- \rightarrow \pi^{-'} + e^{-'} + \pi^0, \quad (14)$$

where an incident high-energy pion scatters inelastically from a target electron in an atomic orbit, as shown in Fig. 1. This reaction and also $K^- + e^- \rightarrow K^{-'} + e^{-'} + \pi^0$ can, in principle, be studied with the (190 - 300) GeV pion and kaon beams in the CERN COMPASS

experiment [23]. New high-statistics pion data will allow for a determination of the form factor for $\pi\gamma^* \rightarrow \pi\pi^0$. The kaon beam three-flavor process can as well test the expected N_c dependence in a low-energy reaction [10, 11].

A similar (pion) experiment has already been performed at the CERN SPS [42]. The experiment did not explicitly extract a value $\mathcal{F}_{3\pi}^{\text{exp}}$ but rather claimed that the experimental value was consistent with theory expectations. Although the experimental backgrounds were described in [42], comparisons of experimental and theoretical distributions versus different kinematic variables were not shown; unfortunately, the data are no longer available for such comparisons [43]. Without presenting such detailed comparisons, Amendolia *et al.* reported 36 events for the reaction $\pi^-e^- \rightarrow \pi^-e^-\pi^0$ corresponding to a cross section of (2.11 ± 0.47) nb. However, without statistical tests such as the Kolmogorov-Smirnov distribution test [44] comparing experimental and theoretical distributions, it is not possible to be sure that background events were not included in the cross section value of Ref. [42]. The cross section of $\pi^-e^- \rightarrow \pi^-e^-\pi^0$, in principle, may also include ρ^- production via the $\pi e \rightarrow \rho e$ transition [45]. However, threshold effects eliminate this background for the 300 GeV pion beam energy of [42], since an energy of $E_\pi \cong 600$ GeV is required to produce a ρ with $m_\rho = 770$ MeV via $\pi e \rightarrow \rho e$.

Our work is organized as follows. In Sec. II we briefly discuss the kinematics and formalism of $\pi^-e^- \rightarrow \pi^-e^-\pi^0$. In Sec. III we present the calculation of the anomaly amplitude $\mathcal{F}_{3\pi}$ within SU(3) ChPT, discuss some phenomenological approaches, and use Monte Carlo techniques to integrate the cross section and compare it with the experimental result of [42]. In Sec. IV we summarize our results and draw some conclusions. Some technical details are relegated to the Appendices.

II. KINEMATICS AND DIFFERENTIAL CROSS SECTION FOR $\pi^-e^- \rightarrow \pi^-e^-\pi^0$

Following the nomenclature of Ref. [46], the kinematics for $a + b \rightarrow 1 + 2 + 3$ is shown in Fig. 1 for an incoming pion that scatters inelastically off an electron target and produces an additional π^0 in the final state: $e^-(p_a) + \pi^-(p_b) \rightarrow e^-(p_1) + \pi^0(p_2) + \pi^-(p_3)$. We consider the target electron to be at rest and the binding energy of the electrons bound in an atom to be negligible relative to the incoming pion energy.

We define the standard set of five invariants as [46]

$$\begin{aligned}
s_1 &\equiv s_{12} = (p_1 + p_2)^2 = (p_a + p_b - p_3)^2, \\
s_2 &\equiv s_{23} = (p_2 + p_3)^2 = (p_a + p_b - p_1)^2, \\
t_1 &\equiv t_{a1} = (p_a - p_1)^2 = (p_2 + p_3 - p_b)^2, \\
t_2 &\equiv t_{b3} = (p_b - p_3)^2 = (p_1 + p_2 - p_a)^2, \\
s &\equiv s_{ab} = (p_a + p_b)^2 = (p_1 + p_2 + p_3)^2.
\end{aligned} \tag{15}$$

The invariant s is fixed by the incident beam energy E_i , $s = M_\pi^2 + m_e^2 + 2E_i m_e$, and one is left with four scalar variables s_1 , s_2 , t_1 , and t_2 .

The fourfold differential cross section, expressed in terms of the five invariants of Eq.

(15), is given by (see, e.g., Ref. [47])²

$$\frac{d\sigma}{ds_1 ds_2 dt_1 dt_2} = \frac{|\overline{\mathcal{M}}|^2}{4(4\pi)^4 \lambda(s, m_e^2, M_\pi^2) (-\Delta_4)^{1/2}}, \quad (16)$$

where

$$\lambda(x, y, z) = x^2 + y^2 + z^2 - 2xy - 2xz - 2yz, \quad (17)$$

and where the Gram determinant is given by [46]

$$\Delta_4 = \frac{1}{16} \begin{vmatrix} 2m_a^2 & 2p_a \cdot p_b & 2p_a \cdot p_1 & 2p_a \cdot p_3 \\ 2p_a \cdot p_b & 2m_b^2 & 2p_b \cdot p_1 & 2p_b \cdot p_3 \\ 2p_a \cdot p_1 & 2p_b \cdot p_1 & 2m_1^2 & 2p_1 \cdot p_3 \\ 2p_a \cdot p_3 & 2p_b \cdot p_3 & 2p_1 \cdot p_3 & 2m_3^2 \end{vmatrix}. \quad (18)$$

The factor 1/16 has been extracted for later convenience. The expressions of the scalar products entering Eq. (18) in terms of the invariants of Eq. (15) are given in Eq. (A1).

In the one-photon exchange approximation (see Fig. 2) the total invariant amplitude \mathcal{M} can be written as

$$\mathcal{M} = -i\mathcal{F}_{3\pi}(s_2, t_2, u_2; q^2) \epsilon^\mu F_\mu, \quad (19)$$

where $\epsilon^\mu = e\bar{u}(p_1)\gamma^\mu u(p_a)/q^2$ is the virtual photon polarization vector ($q = p_a - p_1$) and

$$F_\mu \equiv \epsilon_{\mu\nu\rho\sigma} p_b^\nu p_2^\rho p_3^\sigma. \quad (20)$$

The squared matrix element of Eq. (16) involves the contraction of the standard lepton tensor known from the one-photon exchange approximation in electroproduction processes,

$$\overline{\eta}^{\mu\nu} = \left(2p_a^\mu p_1^\nu + 2p_1^\mu p_a^\nu + q^2 g^{\mu\nu} \right), \quad (21)$$

with the hadronic tensor and is given by

$$|\overline{\mathcal{M}}|^2 = \left(\frac{e}{q^2} \right)^2 |\mathcal{F}_{3\pi}|^2 \overline{\eta}^{\mu\nu} F_\mu F_\nu = \left(\frac{e}{q^2} \right)^2 |\mathcal{F}_{3\pi}|^2 \left(4p_a \cdot F p_1 \cdot F + q^2 F \cdot F \right). \quad (22)$$

The explicit expression for Eq. (22) is given in App. B.

III. THEORETICAL DESCRIPTION OF THE $\mathcal{F}_{3\pi}$ AMPLITUDE

In this section we describe the theoretical input to our analysis of the reaction $\pi^- e^- \rightarrow \pi^- e^- \pi^0$. Since we work in the one-photon exchange approximation, it is sufficient to consider the transition-current matrix element

$$\langle \pi^0(p_2), \pi^-(p_3) | J_\mu(0) | \pi^-(p_b) \rangle = \mathcal{F}_{3\pi}(s_2, t_2, u_2; q^2) \epsilon_{\mu\nu\rho\sigma} p_b^\nu p_2^\rho p_3^\sigma,$$

² Our normalization of the electron states and of the Dirac spinors is given by

$$\langle \vec{p}', s' | \vec{p}, s \rangle = 2E(\vec{p}) (2\pi)^3 \delta^3(\vec{p}' - \vec{p}) \delta_{s's}, \quad \bar{u}(\vec{p}, s') u(\vec{p}, s) = 2m_e \delta_{s's}.$$

where J_μ is the electromagnetic current operator (including the elementary charge). In the isospin-symmetric limit, $\mathcal{F}_{3\pi}$ is a completely symmetric function of the Mandelstam variables s_2 , t_2 , and u_2 . In the *physical* region, the Mandelstam variables satisfy the standard relation $s_2 + u_2 + t_2 = 2M_{\pi^-}^2 + M_{\pi^0}^2 + q^2$. We will lay emphasis on a calculation within the framework of chiral perturbation theory at $\mathcal{O}(p^6)$ but will also discuss the results of some (more) phenomenological approaches. This will allow us to have an estimate of effects which would be subsumed in terms of $\mathcal{O}(p^8)$ and higher.

A. Chiral perturbation theory at $\mathcal{O}(p^6)$

Besides the neutral-pion decay into two photons, the amplitude for $\gamma + \pi^- \rightarrow \pi^0 + \pi^-$ is of prime interest for testing our understanding of anomalous Ward identities. In the momentum and quark-mass expansion, its leading-order contribution is of $\mathcal{O}(p^4)$ and originates from the Wess-Zumino-Witten action [5, 6]. The interaction Lagrangian relevant in the presence of external electromagnetic fields (described by the vector potential \mathcal{A}_μ) is given by [5, 6, 9]

$$\mathcal{L}_{\text{WZW}}^{\text{e.m.}} = -e\mathcal{A}_\mu J^\mu + i\frac{e^2}{16\pi^2}\epsilon^{\mu\nu\rho\sigma}\partial_\nu\mathcal{A}_\rho\mathcal{A}_\sigma\text{Tr}[2Q^2(U\partial_\mu U^\dagger - U^\dagger\partial_\mu U) - QU^\dagger Q\partial_\mu U + QUQ\partial_\mu U^\dagger], \quad (23)$$

where $Q = \text{diag}(2/3, -1/3, -1/3)$ denotes the quark-charge matrix and

$$U = \exp\left(i\frac{\phi}{F_0}\right), \quad \phi = \sum_{a=1}^8 \lambda_a \phi_a, \quad (24)$$

contains the Goldstone boson fields. The current

$$J^\mu = \frac{\epsilon^{\mu\nu\rho\sigma}}{16\pi^2}\text{Tr}(Q\partial_\nu U U^\dagger\partial_\rho U U^\dagger\partial_\sigma U U^\dagger + QU^\dagger\partial_\nu U U^\dagger\partial_\rho U U^\dagger\partial_\sigma U), \quad (25)$$

by itself is not gauge invariant and the additional terms of Eq. (23) are required to obtain a gauge-invariant action. The first term of Eq. (23) gives rise to the $3\phi + \gamma$ coupling (see Fig. 3)

$$\mathcal{L}_{\text{WZW}}^{3\phi+\gamma} = ie\frac{\epsilon^{\mu\nu\rho\sigma}}{8\pi^2 F_0^3}\mathcal{A}_\mu\text{Tr}(Q\partial_\nu\phi\partial_\rho\phi\partial_\sigma\phi), \quad (26)$$

whereas the second is responsible for the $\pi^0 \rightarrow \gamma\gamma$ decay not discussed in this paper.

Weinberg's power counting scheme [7] establishes a connection between the chiral expansion and the loop expansion. Since the anomalous sector only starts at $\mathcal{O}(p^4)$, the contribution at $\mathcal{O}(p^6)$ results from either one-loop diagrams with exactly one vertex from the WZW term or tree-level diagrams with exactly one vertex from the anomalous Lagrangian at $\mathcal{O}(p^6)$. In order to determine the one-loop contributions we need, besides Eq. (23), the WZW contribution involving 5 Goldstone bosons,

$$\mathcal{L}_{\text{WZW}}^{5\phi} = \frac{1}{80\pi^2 F_0^5}\epsilon^{\mu\nu\rho\sigma}\text{Tr}(\phi\partial_\mu\phi\partial_\nu\phi\partial_\rho\phi\partial_\sigma\phi), \quad (27)$$

and the lowest-order Lagrangian in the presence of an electromagnetic field,

$$\mathcal{L}_2 = \frac{F_0^2}{4}\text{Tr}[D_\mu U(D^\mu U)^\dagger] + \frac{F_0^2}{4}\text{Tr}(\chi U^\dagger + U\chi^\dagger), \quad (28)$$

where the relevant covariant derivative is given by $D_\mu U = \partial_\mu U + ie\mathcal{A}_\mu[Q, U]$ and $\chi = 2B_0M$ contains the quark-mass matrix M and B_0 is related to the scalar quark condensate in the chiral limit. The most general anomalous Lagrangian at $\mathcal{O}(p^6)$ has recently been derived in Refs. [31, 32]. According to Table V of Ref. [31], seven structures have the potential of contributing to $3\phi+\gamma$ vertices. In principle, the corresponding low-energy coupling constants should be calculable from the underlying theory. However, since we cannot yet solve QCD, the parameters are either taken as free parameters that are fitted to experimental data or are estimated from models such as meson-resonance saturation [49, 50].

In what follows, we will make use of the SU(3) version of chiral perturbation theory, because this will allow us in future calculations to make contact with other anomalous processes involving in addition kaons. Moreover, we note that previous calculations at $\mathcal{O}(p^6)$ [28] were performed for real photons, $q^2 = 0$, because the amplitude was embedded in a Primakoff reaction, where the virtual photon of the Coulomb field of a heavy nucleus is quasi real. For our reaction such an approximation is not admissible which we will also explicitly see when we discuss the results.

The relevant one-loop diagrams are shown in Figs. 4, 5, and 6 and fall into two distinct groups. The first category just includes one graph (Fig. 4) whose loop is attached to one single vertex (the loop is composed by one internal line so to speak), while in the second category the loop always binds two different vertices together (the loop is therefore composed of two internal lines). Moreover, at $\mathcal{O}(p^6)$ one obtains a contact contribution shown in Fig. 7. Combining the $\mathcal{O}(p^4)$ and $\mathcal{O}(p^6)$ results, multiplying with a factor of $\sqrt{Z_\pi}$ for each external pion line, and renormalizing the coefficients of the $\mathcal{O}(p^6)$ Lagrangian, the result of the one-loop calculation in SU(3) ChPT at $\mathcal{O}(p^6)$ is given by [48]:

$$\begin{aligned} \mathcal{F}_{3\pi}(s_2, t_2, u_2; q^2) = & \frac{e}{4\pi^2 F_\pi^3} \left(1 + C_{M_\pi^2} M_\pi^2 + C_{q^2} q^2 + \frac{1}{32\pi^2 F_\pi^2} \left\{ \frac{s_2 + u_2 + t_2}{3} \ln \left(\frac{\mu^2}{M_\pi^2} \right) \right. \right. \\ & + q^2 \ln \left(\frac{\mu^2}{M_K^2} \right) + \frac{5}{9} (s_2 + u_2 + t_2 + 3q^2) \\ & \left. \left. + \frac{4}{3} [F(s_2, M_\pi^2) + F(t_2, M_\pi^2) + F(u_2, M_\pi^2) + 3F(q^2, M_K^2)] \right\} \right). \quad (29) \end{aligned}$$

The constants $C_{M_\pi^2}$ and C_{q^2} are linear combinations of *renormalized* low-energy coupling constants $\hat{L}_i^{6,\epsilon}$ of the most general odd-intrinsic-parity Lagrangian at $\mathcal{O}(p^6)$ [30, 31, 32, 48],

$$\begin{aligned} C_{M_\pi^2} &= 512\pi^2 (\hat{L}_{13}^{6,\epsilon} - \hat{L}_{14}^{6,\epsilon} - 2\hat{L}_5^{6,\epsilon} - \hat{L}_6^{6,\epsilon}), \\ C_{q^2} &= -\frac{512\pi^2}{3} (\hat{L}_{13}^{6,\epsilon} - \hat{L}_{14}^{6,\epsilon}). \end{aligned} \quad (30)$$

These coefficients still depend on the renormalization scale μ but in such a way that the scale dependence of the logarithms in Eq. (29) is precisely compensated. The function F originates from a standard one-loop integral of mesonic chiral perturbation theory and is given by

$$\begin{aligned} F(a, m^2) &\equiv m^2 \left(1 - \frac{a}{4m^2} \right) J^{(0)} \left(\frac{a}{m^2} \right) - \frac{a}{2}, \\ J^{(0)}(x) &\equiv \int_0^1 dz \ln[1 + x(z^2 - z) - i0^+] \end{aligned}$$

$$= \begin{cases} -2 - \sigma \ln \left(\frac{\sigma-1}{\sigma+1} \right) & (x < 0) \\ -2 + 2\sqrt{\frac{4}{x} - 1} \operatorname{arccot} \left(\sqrt{\frac{4}{x} - 1} \right) & (0 \leq x < 4), \\ -2 - \sigma \ln \left(\frac{1-\sigma}{1+\sigma} \right) - i\pi\sigma & (x > 4) \end{cases}$$

with $\sigma(x) \equiv \sqrt{1 - 4/x}$ for $x \notin [0, 4]$.

Up until now, we have carried out everything which is necessary to meet the requirements of a consistent $\mathcal{O}(p^6)$ calculation within the framework of mesonic ChPT. However, our result still depends on two unknown parameters ($C_{M_\pi^2}$ and C_{q^2}) which prevent us from *predicting* observables such as the total cross section or distributions. Of course, these low-energy coupling constants (LECs) can in principle be determined within appropriate experiments. Here, we actually move on and estimate the constants by using theoretical means which evidently have to go beyond mesonic ChPT. The LECs are supposed to include whatever QCD information on all particles which do not belong to the Goldstone boson octet. At low energies the lightest are expected to be significant and we are thus led to consider the effects due to the vector mesons [49, 50]. For that purpose we made use of the nonlinear chiral Lagrangian of Ref. [51], evaluated the tree-level diagrams contributing to $\gamma^* + \pi^- \rightarrow \pi^0 + \pi^-$ involving internal vector meson lines, and expanded the propagators to be able to collect the arising $\mathcal{O}(p^6)$ pieces (for later purposes we also consider the expressions keeping the full propagators). A comparison (matching) with the polynomial p^6 pieces of the most general anomalous Lagrangian yields the estimate

$$\hat{L}_5^{6,\epsilon} = -\frac{3}{1024\pi^2 m_V^2} = \hat{L}_{13}^{6,\epsilon}, \quad \hat{L}_6^{6,\epsilon} = -\hat{L}_{14}^{6,\epsilon} = 3\hat{L}_5^{6,\epsilon}. \quad (31)$$

Using $m_V = m_\rho = m_\omega$ in SU(3) results in

$$C_{M_\pi^2} = \frac{3}{2m_\rho^2}, \quad C_{q^2} = \frac{2}{m_\rho^2}. \quad (32)$$

Instead of expanding the vector-meson propagators in the vector-meson saturation calculation, we could also keep the complete propagators. This would correspond to the replacement

$$C_{M_\pi^2} M_\pi^2 + C_{q^2} q^2 = \frac{3M_\pi^2 + 4q^2}{2m_\rho^2} \rightarrow \frac{1}{2} \left(\frac{s_2}{m_\rho^2 - s_2} + \frac{t_2}{m_\rho^2 - t_2} + \frac{u_2}{m_\rho^2 - u_2} \right) + \frac{3}{2} \frac{q^2}{m_\omega^2 - q^2} \quad (33)$$

in Eq. (29). We then obtain some estimate of higher-order terms beyond $\mathcal{O}(p^6)$.

A full calculation of all $\mathcal{O}(e^2)$ radiative corrections as well as the isospin symmetry breaking effects due to the different u - and d -quark masses is beyond the scope of the present paper. As discussed in Ref. [35], the most important electromagnetic correction originates from a photon-photon fusion into a neutral pion (see Fig. 8) yielding an additional contribution of the type

$$\Delta\mathcal{F}_{3\pi}^{(e^2)} = \frac{e}{4\pi^2 F_\pi^3} \left(-\frac{2e^2 F_\pi^2}{t_2} \right). \quad (34)$$

Due to the $1/t_2$ pole of the exchanged photon, Eq. (34) becomes important for small values of t_2 . Note that including the single diagram of Fig. 8 does not lead to a conflict with gauge invariance. On the other hand, other electromagnetic corrections were found to be very small in Ref. [35], where the authors concluded that their full calculation can be very well reproduced by adding only the contribution of Eq. (34).

B. Phenomenological approaches

In our analysis we will also compare data with phenomenological calculations using three different forms of the transition-current matrix element:

1. Phenomenological ansatz of Terent'ev [21]:

$$\mathcal{F}_{3\pi}(s_2, t_2, u_2; q^2) = \mathcal{F}_{3\pi}^{(0)} \left[1 + \Delta_\rho \left(\frac{s_2}{m_\rho^2 - s_2} + \frac{t_2}{m_\rho^2 - t_2} + \frac{u_2}{m_\rho^2 - u_2} \right) + \Delta_\omega \frac{q^2}{m_\omega^2 - q^2} \right]. \quad (35)$$

Here, the multiplicative constant $\mathcal{F}_{3\pi}^{(0)}$ refers to the low-energy prediction of Eq. (6) and the variation of the function $\mathcal{F}_{3\pi}$ is supposed to come mainly from vector-meson-exchange diagrams. The parameters Δ_ρ (Δ_ω) implicitly contain factors of $1/\mathcal{F}_{3\pi}^{(0)}$ and are related to the partial widths $\Gamma(\rho^+ \rightarrow \pi^+\pi^0)$ and $\Gamma(\rho \rightarrow \pi\gamma)$ [$\Gamma(\omega \rightarrow e^+e^-)$ and $\Gamma(\omega \rightarrow 3\pi)$]. In the numerical analysis we make use of $m_\rho = 770$ MeV and $m_\omega = 782$ MeV. Comparing Eq. (35) with Eq. (33) would result in $\Delta_\rho \approx 1/2$ and $\Delta_\omega \approx 3/2$ in comparison with $\Delta_\rho \lesssim 1/2$ and $\Delta_\omega \approx 2.6$ of Ref. [21].

2. Pole model of Rudaz including vector-meson dominance (VMD) [42]:

$$\mathcal{F}_{3\pi}(s_2, t_2, u_2; q^2) = \mathcal{F}_{3\pi}^{(0)} \frac{m_\omega^2}{m_\omega^2 - q^2} \frac{m_\rho^2}{3} \left[\frac{1}{m_\rho^2 - s_2} + \frac{1}{m_\rho^2 - t_2} + \frac{1}{m_\rho^2 - u_2} \right]. \quad (36)$$

3. VMD model including the effects of final state p-wave $\pi\pi$ scattering [33]:

$$\begin{aligned} \mathcal{F}_{3\pi}(s_2, t_2, u_2) &= -\frac{1}{2} \frac{e}{4\pi^2 F_\pi^3} \left[1 - \left(\frac{m_\rho^2}{m_\rho^2 - s_2} + \frac{m_\rho^2}{m_\rho^2 - t_2} + \frac{m_\rho^2}{m_\rho^2 - u_2} \right) \right] \\ &\times \left(\frac{1 - s_2/m_\rho^2}{D_1(s_2)} \right) \left(\frac{1 - t_2/m_\rho^2}{D_1(t_2)} \right) \left(\frac{1 - u_2/m_\rho^2}{D_1(u_2)} \right), \end{aligned} \quad (37)$$

where

$$D_1(a) = 1 - \frac{a}{m_\rho^2} - \frac{a}{96\pi^2 F_\pi^2} \ln \left(\frac{m_\rho^2}{M_\pi^2} \right) - \frac{1}{24\pi^2 F_\pi^2} F(a, M_\pi^2). \quad (38)$$

Note that the ansatz of Eq. (37) has only been derived for real photons, $q^2 = 0$, and we therefore have to expect some shortcomings in the description of $\gamma^* + \pi^- \rightarrow \pi^0 + \pi^-$.

C. Results and discussion

Using Monte Carlo techniques we determined the total cross section based on Eq. (16) for kinematical variables inside the region specified by

$$0.0184 \text{ GeV}^2 < s_1 < 0.186 \text{ GeV}^2, \quad (39)$$

$$0.0754 \text{ GeV}^2 < s_2 < 0.325 \text{ GeV}^2, \quad (40)$$

$$-0.236 \text{ GeV}^2 < t_1 < -0.001 \text{ GeV}^2 = t_1^{\text{cut}}, \quad (41)$$

$$-0.269 \text{ GeV}^2 < t_2 < 0, \quad (42)$$

which are the minimal (maximal) values obtained from the equations for the kinematical boundaries [see Ref. [46] and Eq. (C3)]. For the generated invariants the positivity of $-\Delta_4$ of Eq. (16) is checked and events with positive Δ_4 are rejected. In order to check the Monte Carlo calculations we also compared the result with an explicit numerical integration using the simplifications of a constant $\mathcal{F}_{3\pi}$ and $m_e^2 \rightarrow 0$ (see Appendix C).

The results for the total cross section are shown in Table I. The first column denotes the model/theory and the corresponding parameters used; the second column contains the integrated cross section for each case with $\mathcal{F}_{3\pi}^{(0)}$ fixed to $e/(4\pi^2 F_\pi^3) = 9.72 \text{ GeV}^{-3}$. The cases 1), 4), 5), and 6) of Table I were already used in Fig. 4 of Ref. [42] and our corresponding cross sections are in reasonably good agreement. In the third column we show the respective physical threshold amplitudes. In the chiral limit, the threshold amplitudes should reduce to the low-energy prediction $e/(4\pi^2 F_0^3)$ of Eq. (6). In this context it is important to realize that, in general, the dependence of the threshold amplitude on M_π^2 results from both kinematical variables and explicit symmetry breaking. The models of 2) - 6) can only account for the first type of dependence and the corresponding modification is of the type $const. \times M_\pi^2/m_\rho^2$, where the relevant constant depends on the parameters of the model and is of the order of 1. The results of 7) - 11), in addition, contain corrections from Goldstone boson loops of the form $const.' \times M_\pi^2/(4\pi F_\pi)^2$ which are of both kinematical and chiral symmetry breaking type. In the calculation of 9), the $1/t_2$ singularity due to the electromagnetic correction of Eq. (34) generates a 17 % increase in units of $e/(4\pi^2 F_\pi^3)$, but when integrated over t_2 ultimately leads to a less pronounced contribution to the cross section. Finally, in the last column we have also included the overall factor $\mathcal{F}_{3\pi}^{(0)\text{extr}}$ which one extracts based on the experimental result $(2.11 \pm 0.47) \text{ nb}$ of Ref. [42] if one treats $\mathcal{F}_{3\pi}^{(0)}$ as a free parameter in the respective model. The error in $\mathcal{F}_{3\pi}^{(0)\text{extr}}$ only reflects the error in the experimental cross section and does not include any error estimate implied by the models. However, we explicitly do *not* advocate such an extraction as a strict test of the low-energy theorem of Eq. (6), because it introduces a bias in how the chiral limit is approached. Rather, at this point, the only rigorous approach consists of using the chiral expansion as in Eq. (29) and confronting it directly with experimental results.

Using the estimate of Eq. (32) for the parameters $C_{M_\pi^2}$ and C_{q^2} , we obtain as the ChPT result at $\mathcal{O}(p^6)$

$$\sigma = 2.05 \text{ nb.} \quad (43)$$

By also including the most prominent electromagnetic correction [35] in terms of photon-photon fusion into a neutral pion the result increases slightly:

$$\sigma = 2.17 \text{ nb.} \quad (44)$$

Both results are in excellent agreement with the experimental result $(2.11 \pm 0.47) \text{ nb}$ of Ref. [42]. In general, the conceptual advantage of the ChPT calculation over the remaining empirical models is that it is the only calculation which naturally incorporates both genuine quantum effects (loops) and higher-order corrections (as estimated from the VMD saturation). Moreover, in principle, a controlled improvement is possible by performing a complete $\mathcal{O}(p^8)$ calculation, whereas the remaining calculations suffer from the absence of a systematic method of improvement. A comparison of 8) with 7) clearly shows the necessity to include the consequences resulting from the virtuality of the exchanged photon. This can also be seen from the transitions 2) to 3) or 4) to 5) in the calculations using Terent'ev's model. On the other hand, the spread of the obtained cross sections is an indication that

higher-order terms (in the chiral expansion) may play an important role. This conjecture is supported by an analysis for a pion beam energy of 150 GeV which leads to total cross section results between 0.17 nb and 0.21 nb, i.e., the results scatter substantially less than for the higher energy.

In Fig. 9 we show the generated distributions of events as functions of the invariants s_1 , s_2 , t_1 , and t_2 as obtained using chiral perturbation theory at $\mathcal{O}(p^6)$ [see Eq. (29)] with the low-energy constants of Eq. (32) and the most prominent electromagnetic correction of Eq. (34). The results are based on the generation of 100 000 events restricted to the kinematic region

$$\begin{aligned}
2 M_\pi^2 &< s_1 < 10 M_\pi^2, \\
4 M_\pi^2 &< s_2 < 10 M_\pi^2, \\
-0.015 \text{ GeV}^2 &< t_1 < -0.001 \text{ GeV}^2, \\
-0.269 \text{ GeV}^2 &< t_2 < 0.
\end{aligned}
\tag{45}$$

The regions have been chosen such as to avoid the $1/t_1$ pole and to be far enough away from the ρ -meson production threshold. In Fig. 10 we show the differential cross section $d\sigma/dt_1$ as a function of t_1 for three different choices of the low-energy constants of Eq. (32). Clearly, $M_V = 0.2 \text{ GeV}$ (triangles) would correspond to unrealistically large higher-order terms which is supported by the drastically different behavior for this case. Figure 11 illustrates how the inclusion of the electromagnetic correction of Eq. (34) affects the differential cross section $d\sigma/dt_1$. The calculational errors in the plotted points of Figs. 10 and 11 range from 0.1 % at $t_1 = -0.015 \text{ GeV}^2$ to 0.3 % at $t_1 = -0.001 \text{ GeV}^2$. Finally, Fig. 12 contains a comparison of different (model) calculations for the differential cross section $d\sigma/dt_1$. Here, the calculational errors in the plotted points range from 0.03 % at $t_1 = -0.015 \text{ GeV}^2$ to 0.07 % at $t_1 = -0.001 \text{ GeV}^2$.

IV. CONCLUSION

We have studied the reaction $\pi^- e^- \rightarrow \pi^- e^- \pi^0$ with the purpose of obtaining information on the $\gamma\pi \rightarrow \pi\pi$ anomalous amplitude $\mathcal{F}_{3\pi}$. In Table I we have summarized the results of various phenomenological models and of a full calculation at $\mathcal{O}(p^6)$ in chiral perturbation theory for the total cross section using the kinematical conditions of Ref. [42]. In particular, by integrating the ChPT results using Monte Carlo techniques we obtain $\sigma = 2.05 \text{ nb}$ at $\mathcal{O}(p^6)$ and $\sigma = 2.17 \text{ nb}$ after including the dominant electromagnetic correction. Both results are in good agreement with the experimental cross section of $\sigma = (2.11 \pm 0.47) \text{ nb}$ [42]. On the basis of the ChPT results one would extract from the the experimental cross section as amplitudes $\mathcal{F}_{3\pi}^{(0)\text{extr}} = (9.9 \pm 1.1) \text{ GeV}^{-3}$ and $\mathcal{F}_{3\pi}^{(0)\text{extr}} = (9.6 \pm 1.1) \text{ GeV}^{-3}$, respectively, which have to be compared with the low-energy theorem $\mathcal{F}_{3\pi} = e/(4\pi^2 F_\pi^3) = 9.72 \text{ GeV}^{-3}$. We emphasize the need for new data to allow comparison of experimental and theoretical distributions and to obtain $\mathcal{F}_{3\pi}$ with smaller uncertainty. In order to further support our findings and to obtain $\mathcal{F}_{3\pi}$ with a smaller uncertainty, it would be useful for future experiments to also consider distributions such as those shown in Figs. 9 - 12.

Acknowledgments

The work of T. E. and S. S. was supported by the Deutsche Forschungsgemeinschaft (SFB 443). The work of I. G. and M. A. M. was supported by the Israel Science Foundation. Many thanks go to R. Tenchini for interesting clarifications and communications regarding the work Amendolia *et al.*. We also thank A. Vainshtein for helpful comments and encouragement. Furthermore, S. S. would like to thank A. I. L'vov for clarifying comments on the calculation of Appendix C and J. Gasser and J. Gegelia for very useful comments on interpreting the ChPT result.

APPENDIX A: SCALAR PRODUCTS

The ten scalar products appearing in the calculation of the differential cross section of Eq. (16) may be expressed in terms of the five standard invariants of Eq. (15) as [46]

$$\begin{aligned}
2 p_a \cdot p_b &= s - m_a^2 - m_b^2, & 2 p_b \cdot p_2 &= s_2 + t_2 - t_1 - m_3^2, \\
2 p_a \cdot p_1 &= m_a^2 + m_1^2 - t_1, & 2 p_b \cdot p_3 &= m_b^2 + m_3^2 - t_2, \\
2 p_a \cdot p_2 &= s_1 + t_1 - t_2 - m_1^2, & 2 p_1 \cdot p_2 &= s_1 - m_1^2 - m_2^2, \\
2 p_a \cdot p_3 &= s - s_1 + t_2 - m_b^2, & 2 p_1 \cdot p_3 &= s - s_1 - s_2 + m_2^2, \\
2 p_b \cdot p_1 &= s - s_2 + t_1 - m_a^2, & 2 p_2 \cdot p_3 &= s_2 - m_2^2 - m_3^2.
\end{aligned} \tag{A1}$$

APPENDIX B: THE SQUARED AMPLITUDE

In order to evaluate Eq. (22), one makes use of the double epsilon expression

$$\epsilon^{\mu\nu\rho\sigma} \epsilon^{\mu'\nu'\rho'\sigma'} = -\det(g^{\alpha\alpha'}), \quad \alpha = \mu, \nu, \rho, \sigma, \quad \alpha' = \mu', \nu', \rho', \sigma'.$$

The evaluation of the expression in brackets in Eq. (22) is straightforward but tedious and we only quote the final result:

$$\begin{aligned}
&\left(2p_a \cdot F p_1 \cdot F + \frac{1}{2}q^2 F \cdot F\right) \\
&= \left(2p_a \cdot p_1 + \frac{1}{2}q^2\right) [p_b^2(p_2 \cdot p_3)^2 + p_2^2(p_b \cdot p_3)^2 + p_3^2(p_b \cdot p_2)^2 - p_b^2 p_2^2 p_3^2 - 2p_b \cdot p_2 p_b \cdot p_3 p_2 \cdot p_3] \\
&\quad + 2p_a \cdot p_b p_1 \cdot p_b [p_2^2 p_3^2 - (p_2 \cdot p_3)^2] \\
&\quad + 2p_a \cdot p_2 p_1 \cdot p_2 [p_b^2 p_3^2 - (p_b \cdot p_3)^2] \\
&\quad + 2p_a \cdot p_3 p_1 \cdot p_3 [p_b^2 p_2^2 - (p_b \cdot p_2)^2] \\
&\quad + 2(p_a \cdot p_b p_1 \cdot p_2 + p_a \cdot p_2 p_1 \cdot p_b)(p_b \cdot p_3 p_2 \cdot p_3 - p_b \cdot p_2 p_3^2) \\
&\quad + 2(p_a \cdot p_b p_1 \cdot p_3 + p_a \cdot p_3 p_1 \cdot p_b)(p_b \cdot p_2 p_2 \cdot p_3 - p_b \cdot p_3 p_2^2) \\
&\quad + 2(p_a \cdot p_2 p_1 \cdot p_3 + p_a \cdot p_3 p_1 \cdot p_2)(p_b \cdot p_2 p_b \cdot p_3 - p_2 \cdot p_3 p_b^2).
\end{aligned} \tag{B1}$$

We deliberately did not express the scalar products p_b^2 , p_2^2 , and p_3^2 in terms of the masses, because it is then straightforward to apply Eq. (B1) for other processes involving particles with different masses, such as, e.g., $\gamma^*(q) + K^-(p_b) \rightarrow \pi^0(p_2) + K^-(p_3)$. Note that Eq. (B1) is manifestly symmetric under both the exchange $p_1 \leftrightarrow p_a$ and the exchange of any two elements of $\{p_b, p_2, p_3\}$. Finally, using Eqs. (A1) the scalar products in Eq. (B1) may be expressed in terms of the invariant variables of Eq. (15).

APPENDIX C: DIRECT CALCULATION

Using the covariant normalization for both bosons and fermions, the differential cross section for $e^-(p_a) + \pi^-(p_b) \rightarrow e^-(p_1) + \pi^0(p_2) + \pi^-(p_3)$ can be written as

$$d\sigma = \frac{1}{4} \frac{1}{\sqrt{(p_a \cdot p_b)^2 - m_e^2 M_\pi^2}} \frac{1}{(2\pi)^5} |\mathcal{M}|^2 \delta^4(p_a + p_b - p_1 - p_2 - p_3) \frac{d^3 p_1}{2E_1} \frac{d^3 p_2^*}{2E_2^*} \frac{d^3 p_3^*}{2E_3^*}, \quad (\text{C1})$$

where we consider the final-state pions in their rest frame (denoted by $*$) and the ejected electron in the laboratory frame. Integration with respect to \vec{p}_3^* and E_2^* yields

$$d\sigma = \frac{1}{4} \frac{1}{\sqrt{(p_a \cdot p_b)^2 - m_e^2 M_\pi^2}} \frac{1}{(2\pi)^5} |\mathcal{M}|^2 \frac{d^3 p_1}{2E_1} \frac{|\vec{p}_2^*| d\Omega_2^*}{4\sqrt{s_2}}.$$

Let the pion beam define the positive z axis. Using

$$\int_0^{2\pi} \frac{d^3 p_1}{E_1} = \pi dE_1 dp_{1z}$$

in combination with

$$\begin{aligned} 2|\vec{p}_b|p_{1z} &= s_2 - M_\pi^2 - \frac{t_1}{2m_e^2}(m_e^2 + s - M_\pi^2), \\ 2m_e E_1 &= 2m_e^2 - t_1, \\ m_e |\vec{p}_p| &= \sqrt{(p_a \cdot p_b)^2 - m_e^2 M_\pi^2}, \end{aligned}$$

we obtain

$$\pi dE_1 dp_{1z} = \frac{\pi}{4} \frac{dt_1 ds_2}{\sqrt{(p_a \cdot p_b)^2 - m_e^2 M_\pi^2}}$$

and can thus write

$$d\sigma = \frac{1}{4} \frac{1}{\sqrt{(p_a \cdot p_b)^2 - m_e^2 M_\pi^2}} \frac{1}{(2\pi)^5} |\mathcal{M}|^2 \frac{\pi dt_1 ds_2}{4\sqrt{(p_a \cdot p_b)^2 - m_e^2 M_\pi^2}} \frac{|\vec{p}_2^*| d\Omega_2^*}{4\sqrt{s_2}}. \quad (\text{C2})$$

To obtain the kinematic boundaries of s_2 and t_1 one can either solve for t_1 in terms of s_2 , or vice versa [46],

$$\begin{aligned} t_1^\pm &= m_a^2 + m_1^2 - \frac{1}{2s} [(s + m_a^2 - m_b^2)(s - s_2 + m_1^2) \mp \lambda^{1/2}(s, m_a^2, m_b^2) \lambda^{1/2}(s, s_2, m_1^2)], \\ s_2^\pm &= s + m_1^2 - \frac{1}{2m_a^2} [(s + m_a^2 - m_b^2)(m_a^2 + m_1^2 - t_1) \mp \lambda^{1/2}(s, m_a^2, m_b^2) \lambda^{1/2}(t_1, m_a^2, m_1^2)], \end{aligned} \quad (\text{C3})$$

where $\lambda(x, y, z)$ is defined in Eq. (17).

In order to test our numerical integration programs, we evaluated Eq. (C2) under the following simplifying assumptions: We neglected terms containing the square of the electron

mass and we assumed $\mathcal{F}_{3\pi}$ to be constant [see Eq. (6)]. Under these assumptions we obtain for the angular integral

$$\int d\Omega_2^*(4p_a \cdot F p_1 \cdot F + t_1 F \cdot F) = -\frac{\pi}{6} t_1 (s_2 - 4M_\pi^2) [t_1^2 + 2t_1(s - s_2 - M_\pi^2) + (s - M_\pi^2)^2 + (s - s_2)^2]. \quad (\text{C4})$$

Inserting Eq. (C4) into Eq. (C2) and using Eq. (22) results in

$$\frac{d\sigma}{dt_1 ds_2} = -\frac{1}{6144\pi^3} \frac{1}{(s - M_\pi^2)^2} |e\mathcal{F}_{3\pi}|^2 \frac{(s_2 - 4M_\pi^2)^{3/2}}{\sqrt{s_2 t_1}} [t_1^2 + 2t_1(s - s_2 - M_\pi^2) + (s - M_\pi^2)^2 + (s - s_2)^2] \quad (\text{C5})$$

for $m_e^2 \rightarrow 0$ and $\mathcal{F}_{3\pi} = \text{const.}$ We first integrate Eq. (C5) with respect to t_1 from $t_1^- = -(s - M_\pi^2)(s - s_2)/s$ to $t_1^+ = t_1^c$, where t_1^c is an experimental cut on the maximal value of t_1 :

$$\int_{t_1^-}^{t_1^c} dt_1 \frac{d\sigma}{dt_1 ds_2} = \frac{1}{6144\pi^3} \frac{1}{(s - M_\pi^2)^2} |e\mathcal{F}_{3\pi}|^2 \frac{(s_2 - 4M_\pi^2)^{3/2}}{\sqrt{s_2}} \times \left[\frac{1}{2}(t_1^{-2} - t_1^{c2}) + 2(s - s_2 - M_\pi^2)(t_1^- - t_1^c) + [(s - M_\pi^2)^2 + (s - s_2)^2] \ln \left(\frac{t_1^-}{t_1^c} \right) \right], \quad (\text{C6})$$

where $4M_\pi^2 \leq s_2 \leq s_2^c = s[1 + t_1^c/(s - M_\pi^2)]$ as implied by the physical boundary conditions. A numerical integration of

$$\sigma(t_1^c) = \int_{4M_\pi^2}^{s_2^c} ds_2 \int_{t_1^-}^{t_1^c} dt_1 \frac{d\sigma}{dt_1 ds_2} \quad (\text{C7})$$

yields $\sigma(t_1^c) = 1.864$ nb for $t_1^c = -0.001$ GeV² which agrees within less than 0.5 % with the Monte Carlo result 1.855 nb (we used $M_\pi = 139.57$ MeV).

-
- [1] S. L. Adler, Phys. Rev. **177**, 2426 (1969).
 - [2] S. L. Adler and W. A. Bardeen, Phys. Rev. **182**, 1517 (1969).
 - [3] W. A. Bardeen, Phys. Rev. **184**, 1848 (1969).
 - [4] J. S. Bell and R. Jackiw, Nuovo Cim. A **60**, 47 (1969).
 - [5] J. Wess and B. Zumino, Phys. Lett. B **37**, 95 (1971).
 - [6] E. Witten, Nucl. Phys. **B223**, 422 (1983).
 - [7] S. Weinberg, Physica A **96**, 327 (1979); J. Gasser and H. Leutwyler, Annals Phys. **158**, 142 (1984); Nucl. Phys. **B250**, 465 (1985).
 - [8] A. Pich, Rept. Prog. Phys. **58**, 563 (1995); A. Pich, in *Probing the Standard Model of Particle Interactions*, Proceedings of the Les Houches Summer School in Theoretical Physics, Session 68, Les Houches, France, 28 July - 5 September 1997, edited by R. Gupta, A. Morel, E. de Rafael, and F. David (Elsevier, Amsterdam, 1999); G. Ecker, Lectures given at Advanced School on Quantum Chromodynamics (QCD 2000), Benasque, Huesca, Spain, 3 - 6 July 2000, hep-ph/0011026.
 - [9] S. Scherer, in *Advances in Nuclear Physics, Vol. 27*, edited by J. W. Negele and E. W. Vogt (Kluwer Academic/Plenum Publishers, New York, 2003).

- [10] O. Bär and U.-J. Wiese, Nucl. Phys. **B609**, 225 (2001).
- [11] R. N. Rogalyov, hep-ph/0202046.
- [12] B. Borasoy and E. Lipartia, Phys. Rev. D **71**, 014027 (2005).
- [13] S. Eidelman et al., Phys. Lett. B **592**, 1 (2004).
- [14] J. F. Donoghue, B. R. Holstein, and Y. C. Lin, Phys. Rev. Lett. **55**, 2766 (1985).
- [15] J. Bijnens, A. Bramon, and F. Cornet, Phys. Rev. Lett. **61**, 1453 (1988).
- [16] B. Moussallam, Phys. Rev. D **51**, 4939 (1995).
- [17] B. Ananthanarayan and B. Moussallam, JHEP **0205**, 052 (2002).
- [18] N. F. Nasrallah, Phys. Rev. D **66**, 076012 (2002).
- [19] J. L. Goity, A. M. Bernstein, and B. R. Holstein, Phys. Rev. D **66**, 076014 (2002).
- [20] A. Gasparian *et al.*, Conceptual design report *A Precision Measurement of the Neutral Pion Lifetime via the Primakoff Effect*, url: www.jlab.org/primex.
- [21] M. V. Terent'ev, Phys. Lett. B **38**, 419 (1972).
- [22] Yu. M. Antipov *et al.*, Phys. Rev. D **36**, 21 (1987).
- [23] G. Baum *et al.* (COMPASS Collaboration), Proposal for a *Common Muon and Proton Apparatus for Structure and Spectroscopy*, CERN-SPSLC 96-14, SPSC/P 297; <http://wwwcompass.cern.ch>.
- [24] M. A. Moinester and V. Steiner, *Primakoff physics for CERN COMPASS hadron beam: Hadron polarizabilities, hybrid mesons, chiral anomaly, meson radiative transitions*, contributed to Charles U./JINR and International U. (Dubna) CERN COMPASS Summer School, August 1997, Prague, Czech Republic, hep-ex/9801011.
- [25] M. A. Moinester (COMPASS Collaboration), *Pion and kaon polarizabilities at CERN COMPASS*, contributed to Advanced Study Institute on Symmetries and Spin (Paha SPIN 2002), Prague, Czech Republic, 14-27 July 2002, Czech. J. Phys. **53**, B169 (2003), hep-ex/0301024.
- [26] M. A. Moinester, *Hybrid Meson Production via Pion Scattering from the Nuclear Coulomb Field*, Proceedings of the "Future Physics at COMPASS" Workshop, Geneva, Switzerland, Sept. 2002, CERN Yellow Report 2004-011, http://wwwcompass.cern.ch/compass/publications/2004_yellow/, hep-ex/0301023.
- [27] J. Bijnens, A. Bramon, and F. Cornet, Z. Phys. C **46**, 599 (1990).
- [28] J. Bijnens, A. Bramon and F. Cornet, Phys. Lett. B **237**, 488 (1990).
- [29] J. Bijnens, Int. J. Mod. Phys. A **8**, 3045 (1993).
- [30] D. Issler, SLAC-PUB-4943-REV (1990) (unpublished); R. Akhoury and A. Alfakih, Annals Phys. **210**, 81 (1991); H. W. Fearing and S. Scherer, Phys. Rev. D **53**, 315 (1996).
- [31]
- [31] T. Ebertshäuser, H. W. Fearing, and S. Scherer, Phys. Rev. D **65**, 054033 (2002).
- [32]
- [32] J. Bijnens, L. Girlanda, and P. Talavera, Eur. Phys. J. C **23**, 539 (2002).
- [33] B. R. Holstein, Phys. Rev. D **53**, 4099 (1996).
- [34] T. Hannah, Nucl. Phys. **B593**, 577 (2001).
- [35] L. Ametller, M. Knecht, and P. Talavera, Phys. Rev. D **64**, 094009 (2001).
- [36] T. N. Truong, Phys. Rev. D **65**, 056004 (2002).
- [37] R. Alkofer and C. D. Roberts, Phys. Lett. B **369**, 101 (1996); B. Bistrovic and D. Klabucar, Phys. Rev. D **61**, 033006 (2000); B. Bistrovic and D. Klabucar, Phys. Lett. B **478**, 127 (2000); X. y. Li and Y. Liao, Phys. Lett. B **505**, 119 (2001); S. R. Cotanch and P. Maris, Phys. Rev. D **68**, 036006 (2003).
- [38] M. A. Moinester, in *Proceedings of the International Conference On Physics With GeV Particle*

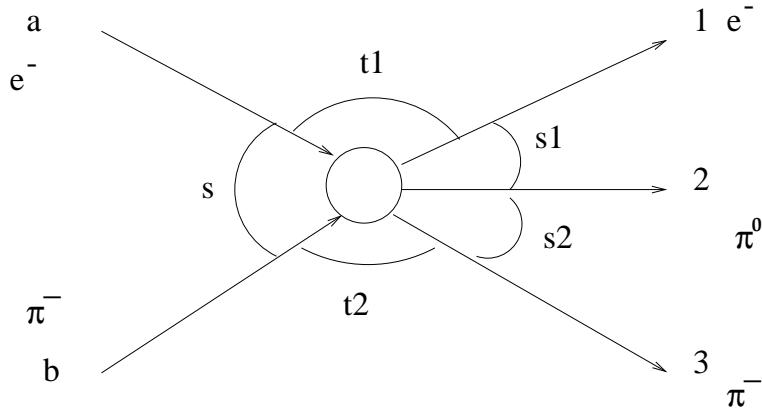


FIG. 1: Kinematics of the reaction $e^-(p_a) + \pi^-(p_b) \rightarrow e^-(p_1) + \pi^0(p_2) + \pi^-(p_3)$.

Beams, 22 - 25 August 1994, Jülich, Germany, edited by H. Machner and K. Sistemich (World Scientific, Singapore, 1995), hep-ph/9409307.

- [39] R. A. Miskimen, K. Wang, A. Yegneswaran (spokespersons), Thomas Jefferson National Accelerator Facility Experiment E94015, *Study of the Axial Anomaly using the $\gamma\pi^+ \rightarrow \pi^+\pi^0$ Reaction Near Threshold*.
- [40] B. Asavapibhop, *Study of the Axial Anomaly in the $\gamma p \rightarrow \pi^+\pi^0 n$ Reaction at Low t Using the CLAS and the Photon Tagger*, PhD thesis, University of Massachusetts, Amherst, Massachusetts, 2000, http://www.jlab.org/Hall-B/clas_g1/anomaly/.
- [41] R. A. Miskimen, private communication.
- [42] S. R. Amendolia *et al.*, Phys. Lett. B **155**, 457 (1985).
- [43] R. Tenchini (CERN), private communication.
- [44] W. H. Press, B. P. Flannery, S. A. Teukolsky, W. T. Vetterling, *Numerical Recipes in Fortran: The Art of Scientific Computing (2nd Edn.)* (Cambridge University Press, Cambridge, 1992).
- [45] J. M. LoSecco, Phys. Rev. D **51**, 6572 (1995).
- [46] E. Byckling and K. Kajantie, *Particle Kinematics* (Wiley, New York, 1973).
- [47] C. Unkmeir, A. Ocherashvili, T. Fuchs, M. A. Moinester, and S. Scherer, Phys. Rev. C **65**, 015206 (2002).
- [48] T. Ebertshäuser, *Mesonic Chiral Perturbation Theory: Odd Intrinsic Parity Sector*, PhD thesis, Johannes Gutenberg-Universität, Mainz, Germany, 2001, <http://archimed.uni-mainz.de/>; T. Ebertshäuser and S. Scherer, in preparation.
- [49] G. Ecker, J. Gasser, H. Leutwyler, A. Pich, and E. de Rafael, Phys. Lett. B **223**, 425 (1989).
- [50] G. Ecker, J. Gasser, A. Pich, and E. de Rafael, Nucl. Phys. **B321**, 311 (1989).
- [51] T. Fujiwara, T. Kugo, H. Terao, S. Uehara, and K. Yamawaki, Prog. Theor. Phys. **73**, 926 (1985).

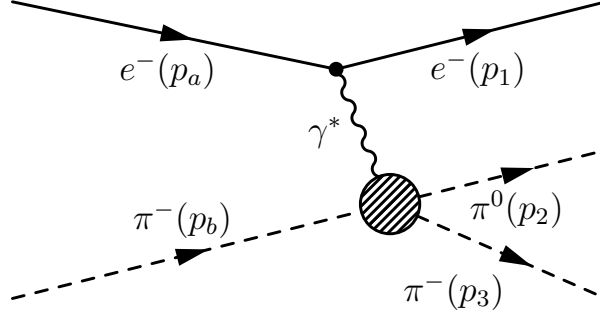


FIG. 2: One-photon exchange approximation of the reaction $e^-(p_a) + \pi^-(p_b) \rightarrow e^-(p_1) + \pi^0(p_2) + \pi^-(p_3)$.

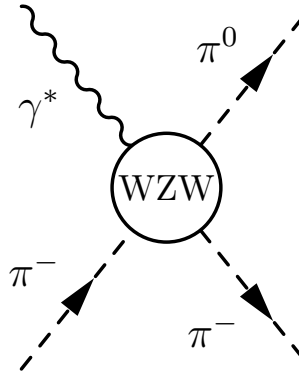


FIG. 3: WZW diagram obtained from Eq. (26).

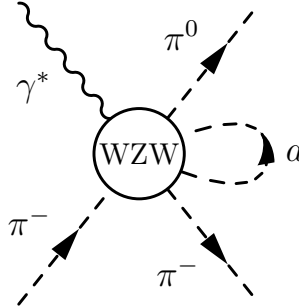


FIG. 4: One-loop diagram obtained from expanding the first term of Eq. (23) to fifth order in the Goldstone boson fields and contracting two lines to form a loop.

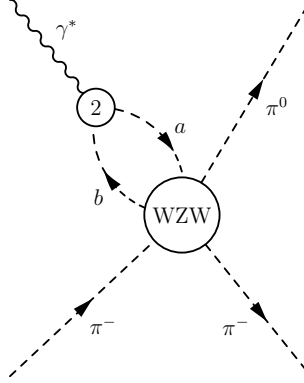


FIG. 5: One-loop diagram obtained from contracting two lines of Eq. (27) with the two lines of the $2\phi + \gamma$ vertex from \mathcal{L}_2 to form a loop.

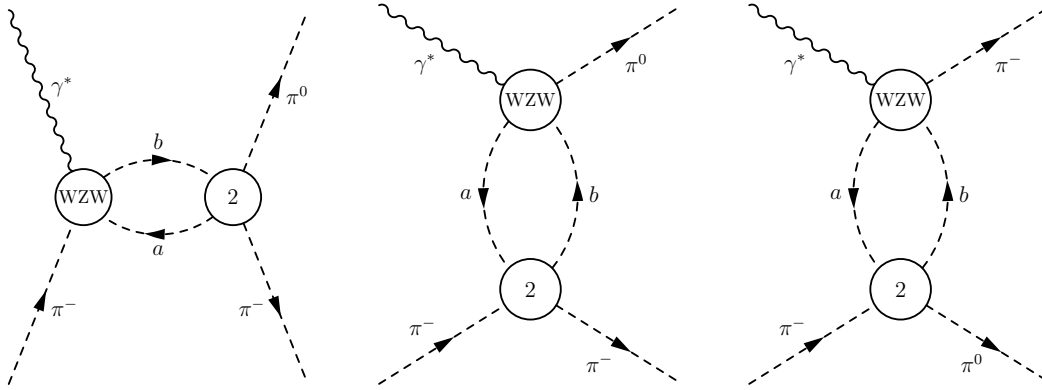


FIG. 6: One-loop diagrams obtained from contracting two lines of Eq. (26) with two lines of the 4ϕ vertex from \mathcal{L}_2 to form a loop (cuts in the s_2 , t_2 , and u_2 channels, respectively).

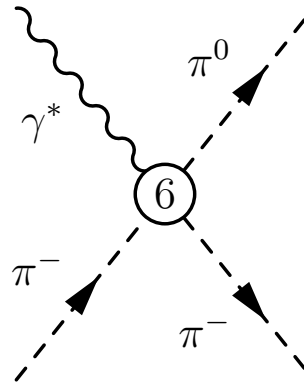


FIG. 7: Contact diagram obtained from \mathcal{L}_6 .

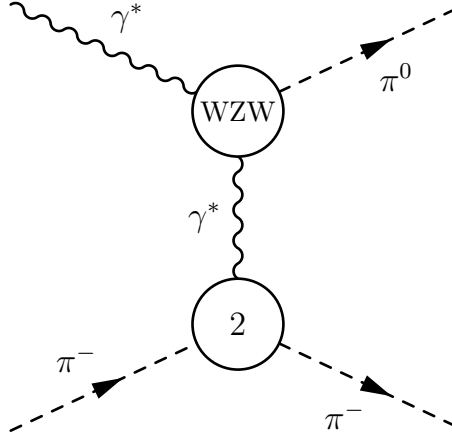


FIG. 8: Electromagnetic correction.

TABLE I: Total cross section for $\pi^-e^- \rightarrow \pi^-e^-\pi^0$ as obtained in different models and chiral perturbation theory (see text). The third column contains the physical threshold amplitudes for $q^2 = 0$. In the last column we made use of the experimental result (2.11 ± 0.47) nb of Ref. [42] to convert this into the value for $\mathcal{F}_{3\pi}^{(0)\text{extr}}$ which would be extracted based on the given model: $\mathcal{F}_{3\pi}^{(0)\text{extr}} = 9.72 \sqrt{\sigma_{\text{exp}}/\sigma_{\text{model}}} \text{ GeV}^{-3}$. Here we follow the common practice to quote the extracted values. The error only reflects the experimental error and does not include any error estimate implied by the models. We stress that in the framework of ChPT the overall factor of Eq. (29) is not a free parameter. Therefore, the “extracted” values for the ChPT calculation have to be taken with a grain of salt (see the discussion in the text).

Model/theory	cross section [nb]	$\mathcal{F}_{3\pi}^{\text{thr}}$ [GeV ⁻³]	$\mathcal{F}_{3\pi}^{(0)\text{extr}}$ [GeV ⁻³]
1) $\mathcal{F}_{3\pi} = \frac{e}{4\pi^2 F_\pi^3} = 9.72 \text{ GeV}^{-3}$	1.92	9.7	10.2 ± 1.1
2) Terent'ev, Eq. (35) with $\Delta_\rho = 0.5$ and $\Delta_\omega = 0$	2.80	10.3	8.4 ± 0.9
3) Terent'ev, Eq. (35) with $\Delta_\rho = 0.5$ and $\Delta_\omega = 1.5$	2.62	10.3	8.7 ± 1.0
4) Terent'ev, Eq. (35) with $\Delta_\rho = 0.35$ and $\Delta_\omega = 0$	2.51	10.1	8.9 ± 1.0
5) Terent'ev, Eq. (35) with $\Delta_\rho = 0.35$ and $\Delta_\omega = 3.2$	2.18	10.1	9.6 ± 1.1
6) Rudaz, Eq. (36)	2.36	10.0	9.2 ± 1.0
7) ChPT at $\mathcal{O}(p^6)$ [Eq. (29)] without q^2 dependence	2.33	10.4	9.2 ± 1.0
8) ChPT at $\mathcal{O}(p^6)$ [Eq. (29)] with q^2 dependence	2.05	10.4	9.9 ± 1.1
9) ChPT at $\mathcal{O}(p^6)$ [Eq. (29)] with q^2 dependence plus electromagnetic correction of Eq. (34)	2.17	12.1	9.6 ± 1.1
10) ChPT at $\mathcal{O}(p^6)$ with modified dependence of Eq. (33)	2.83	10.5	8.4 ± 0.9
11) Holstein, Eq. (37)	3.05	10.4	8.1 ± 0.9

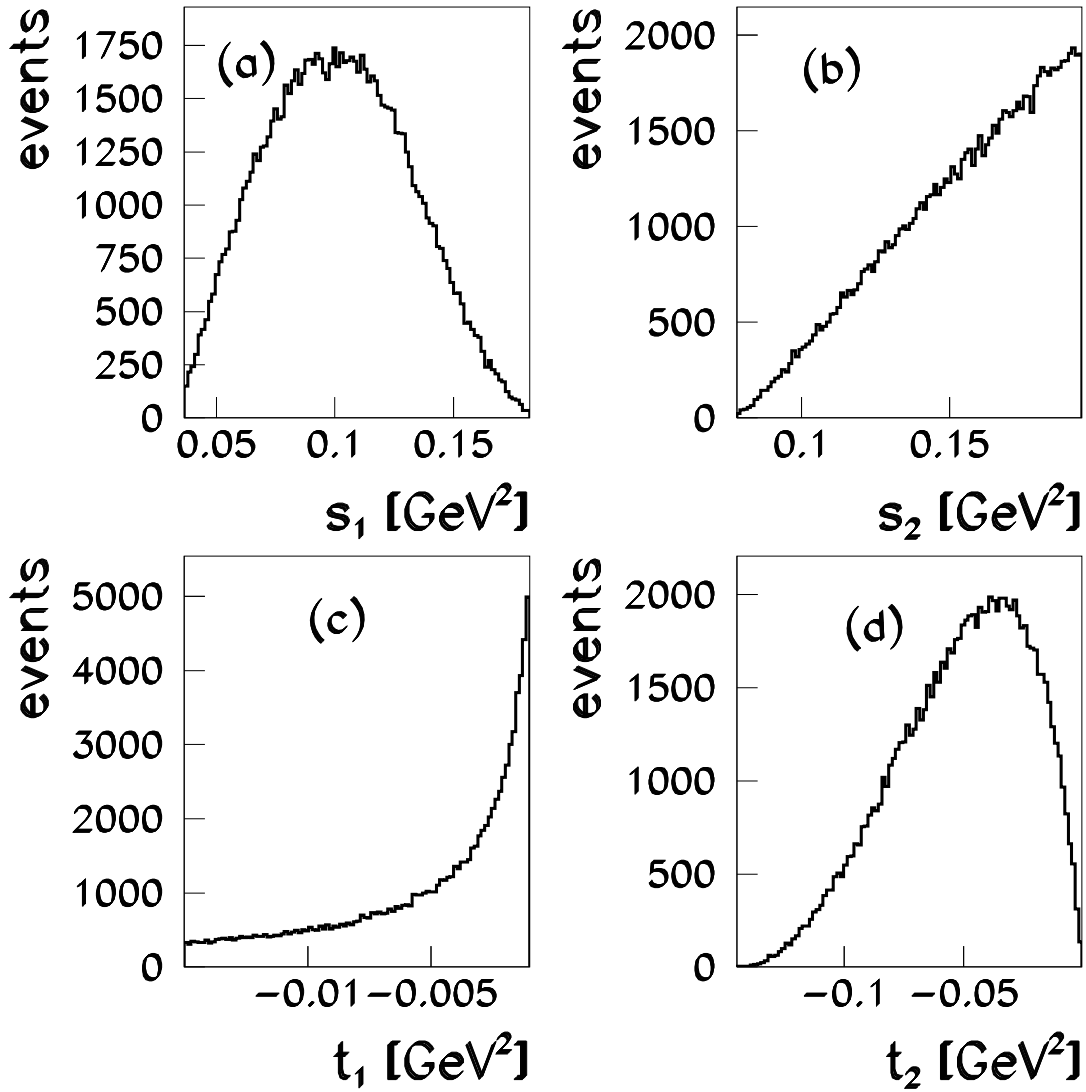


FIG. 9: The distributions of events as functions of the invariants (a) s_1 , (b) s_2 , (c) t_1 , and (d) t_2 as obtained using chiral perturbation theory at $\mathcal{O}(p^6)$ [see Eq. (29)] with the low-energy constants of Eq. (32) and including the most prominent electromagnetic correction of Eq. (34).

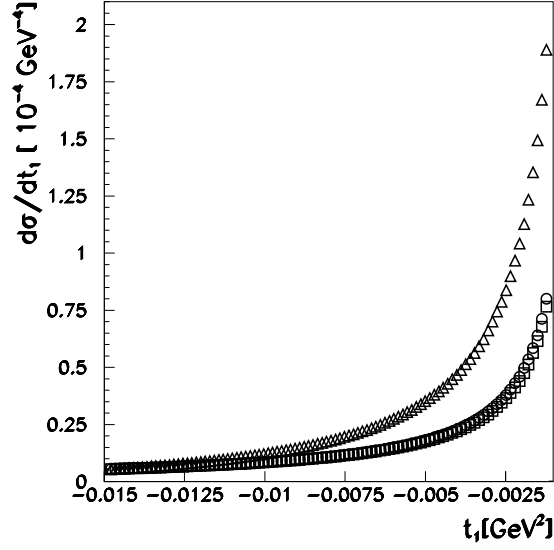


FIG. 10: Differential cross section $d\sigma/dt_1$ as a function of t_1 using chiral perturbation theory at $\mathcal{O}(p^6)$ [see Eq. (29)] including the most prominent electromagnetic correction of Eq. (34). The low-energy constants of Eq. (32) have been fixed using $M_V = 0.2$ GeV (triangles), $M_V = m_\rho$ (circles), and $M_V = 2m_\rho$ (squares), respectively.

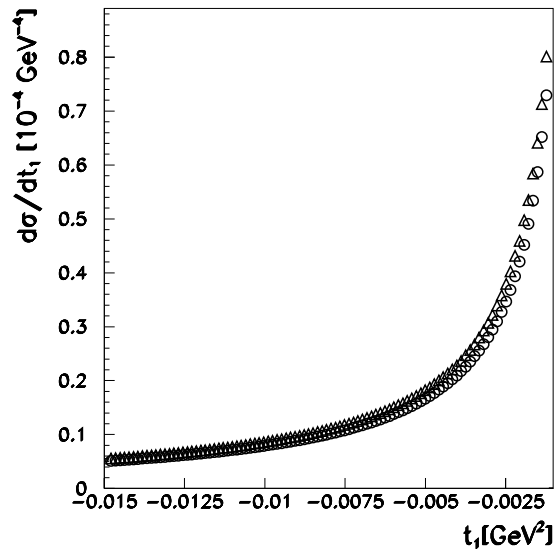


FIG. 11: Differential cross section $d\sigma/dt_1$ as a function of t_1 using chiral perturbation theory at $\mathcal{O}(p^6)$ [see Eq. (29)] with the low-energy constants of Eq. (32) without (circles) and including (triangles) the most prominent electromagnetic correction of Eq. (34).

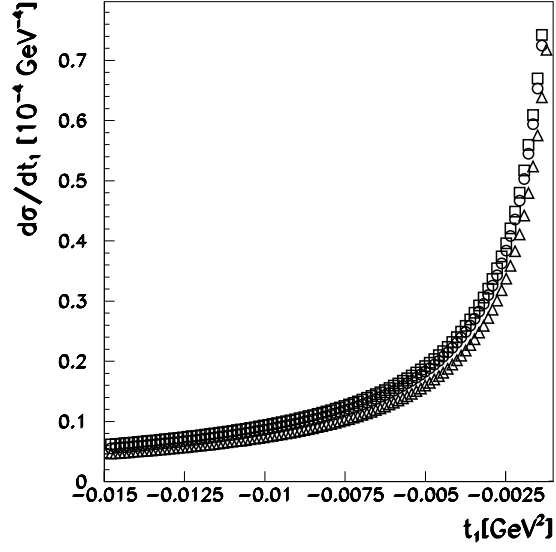


FIG. 12: Differential cross section $d\sigma/dt_1$ as a function of t_1 for the model of Terent'ev, Eq. (35) with $\Delta_\rho = 0.35$ and $\Delta_\omega = 3.2$ (triangles), ChPT at $\mathcal{O}(p^6)$ [Eq. (29)] plus electromagnetic correction of Eq. (34) (circles), and the model of Holstein, Eq. (37) (squares).